Journal of Hydrology 544 (2017) 467–478

Contents lists available at ScienceDirect

Journal of Hydrology

journal homepage: www.elsevier.com/locate/jhydrol

Research papers

Two-dimensional vertical moisture-pressure dynamics above groundwater waves: Sand flume experiments and modelling

Seyed Mohammad Hossein Jazayeri Shoushtari [a,*], Nick Cartwright [a], Pierre Perrochet [b], Peter Nielsen [c]

[a] Griffith School of Engineering, Gold Coast Campus, Griffith University, Queensland 4222, Australia
[b] Centre d'hydrogéologie, Rue Emile-Argand 11, Case postale 158, 2009 Neuchâtel, Switzerland
[c] School of Civil Engineering, The University of Queensland, 4072, Australia

ARTICLE INFO

Article history:
Received 13 May 2016
Received in revised form 22 November 2016
Accepted 28 November 2016
Available online 29 November 2016
This manuscript was handled by Corrado Corradini, Editor-in-Chief, with the assistance of Stephen Worthington, Associate Editor

Keywords:
Groundwater
Hysteresis
Richards' equation
Oscillatory flow
Unsaturated flow

ABSTRACT

This paper presents a new laboratory dataset on the moisture-pressure relationship above a dispersive groundwater wave in a two-dimensional vertical unconfined sand flume aquifer driven by simple harmonic forcing. A total of five experiments were conducted in which all experimental parameters were kept constant except for the oscillation period, which ranged from 268 s to 2449 s between tests. Moisture content and suction head sensor pairings were co-located at two locations in the unsaturated zone both approximately 0.2 m above the mean watertable elevation and respectively 0.3 m and 0.75 m from the driving head boundary. For all oscillation periods except for the shortest ($T = 268$ s), the formation of a hysteretic moisture-pressure scanning loop was observed. Consistent with the decay of the saturated zone groundwater wave, the size of the observed moisture-pressure scanning loops decayed with increasing distance landward and the decay rate is larger for the shorter oscillation periods. At the shortest period ($T = 268$ s), the observed moisture-pressure relationship was observed to be non-hysteretic but with a capillary capacity that differs from that of the static equilibrium wetting and drying curves. This finding is consistent with observations from existing one-dimensional vertical sand column experiments. The relative damping of the moisture content with distance landward is higher than that for the suction head consistent with the fact that transmission of pressure through a porous medium occurs more readily than mass transfer. This is further supported by the fact that observed phase lags for the unsaturated zone variables (i.e. suction head and moisture content) relative to the driving head are greater than the saturated zone variables (i.e. piezometric head). Harmonic analysis of the data reveals no observable generation of higher harmonics in either moisture or pressure despite the strongly non-linear relationship between the two. In addition, a phase lag of moisture content relative to the suction head was observed indicating that the response time of the moisture content to watertable motion is greater than that of the pore water pressure. The observed moisture-pressure dynamics are qualitatively reproduced using a hysteretic Richards' equation model. However, quantitative differences exist which are likely to be due to previous findings that demonstrated that the Richards' equation model is unable to accurately reproduce the observed watertable wave dispersion, particularly at shorter period oscillations.

1. Introduction

Watertable dynamics play an important role in a variety of coastal zone processes such as salt-water intrusion and contaminant transport into coastal aquifers (e.g. Xin et al., 2010; Robinson et al., 2006) and beach profile morphology (e.g. Emery and Foster, 1948; Grant, 1946, 1948, Bakhtyar et al., 2011). The influence of the unsaturated zone on watertable dynamics has been examined from a range of perspectives including: application of the Green and Ampt (1911) parameterization of the capillary fringe (e.g. Barry et al., 1996; Li et al., 2000); field investigations (e.g. Heiss et al., 2014); laboratory sand column experiments (e.g. Lehmann et al., 1998; Nielsen and Perrochet, 2000a,b; Stauffer and Kinzelbach, 2001) and numerical studies (e.g. Clement et al., 1994). To date, only a limited number of observations of the moisture-pressure dynamics above an oscillating watertable have been made and all of these have been made using a one-dimensional vertical (1DV) sand column.

* Corresponding author.
E-mail address: a.jazayerishoushtari@griffith.edu.au (S.M.H.J. Shoushtari).

http://dx.doi.org/10.1016/j.jhydrol.2016.11.060
0022-1694/

Lehmann et al. (1998) conducted sand column experiments to describe water content variations due to water pressure fluctuations at the bottom of the sand column. Water content and potential were measured at different soil depths and an increase in water content, potential damping and time lag by increasing the distance from the capillary fringe was observed. Damping in watertable dynamics due to hysteresis and a highly asymmetrical response of water content to symmetrical fluctuation at the bottom boundary was also noted. They solved a 1DV Richards' equation using the HYSTFLOW (Stauffer, 1996) code with the Brooks and Corey (1966) formulas for the water retention curves, and a modified Mualem (1984) hysteresis model. The hysteretic model was able to reproduce the measured average water content better than non-hysteretic models. Although the hysteretic simulations for the moisture content and the matric potential were close to measured values in or near the capillary fringe, the hysteretic model underestimated the damping in the water content and the matric potential under highly unsaturated conditions above the capillary fringe. Stauffer and Kinzelbach (2001) also formulated a 1DV model for saturated/unsaturated flow based on Richards' equation and Mualem's (1984) hysteresis model which compared well with their sand column observations of moisture content measured using gamma probes.

Nielsen and Perrochet (2000a,b) measured watertable heights and total moisture content in a sand column subjected to a simple harmonic driving head at the bottom of the column with oscillation periods ranging from 14.5 min to 6.5 h. They observed that the watertable height responded very closely to the driving head while total moisture content varied very little compared with the watertable height. Based on the observed frequency response function of the total moisture content relative to the watertable, Nielsen and Perrochet (2000a,b) proposed a complex effective porosity (n_d) concept which implicitly accounts for any hysteresis effects on watertable motion. The magnitude $|n_d|$ accounts for the damping of the total moisture relative to the watertable motion and the argument ($-Arg(n_d)$) describes the phase shift between watertable height and total water content. They also compared experimental data with numerical results of Richards' equation with van Genuchten model (van Genuchten, 1980) and found that the non-hysteretic Richards' model failed to represent experimental data of watertable height and total water content. Nielsen and Perrochet (2000a,b) suggested that considering hysteresis dynamics can improve the Richards' model results.

Werner and Lockington (2003) modelled the sand column data of Nielsen and Perrochet (2000a,b) using a modified version of HYDRUS 1D (Šimůnek et al., 1998) with the hysteresis algorithms of Parker and Lenhard (1987). Inclusion of hysteresis effects provided an improved model-data comparison (in terms of the watertable frequency response function) than was achieved with a non-hysteretic model. Whilst Werner and Lockington (2003) examined the nature of the moisture-pressure scanning loops numerically, none of the above studies have observed the nature of these loops using a physical model.

Cartwright (2014) conducted sand column experiments to study the moisture-pressure dynamics above an oscillating watertable with periods ranging from 10 s to 12.5 h. Using co-located moisture and pressure measurements, their data show clear formation of hysteretic scanning loops for the longer period while for periods less than 15 min, the observed moisture-pressure dynamics became non-hysteretic. The general slope of the observed scanning loops (the capillary capacity) for the high-frequency periods is close to non-hysteretic van Genuchten (1980) curve with $\beta = 3$ which explained the prediction capability of non-hysteretic Richards' model in previous sand column experiments for high frequency watertable motion (Cartwright et al., 2005).

Cartwright (2014) then used the HYDRUS 1D model (Šimůnek et al., 1998) to solve the Richards' equation numerically in conjunction with the van Genuchten moisture retention curves and the empirical hysteresis model of Scott et al. (1983). Despite known artificial pumping errors associated with Scott's et al. (1983) hysteresis model (Werner and Lockington, 2003), the model was able to qualitatively reproduce the observed scanning loops with only some quantitative discrepancies which are likely due to the uncertainty in assumed model parameters.

All of the above mentioned studies only considered a 1DV sand column system and to date, moisture-pressure dynamics above a two-dimensional vertical (2DV) propagating watertable wave are yet to be studied. This paper aims to fill this knowledge gap and presents a new 2DV laboratory dataset to bring to light insights into the moisture-pressure dynamics above a propagating watertable wave. The data is also used to evaluate the predictive capability of a 2DV hysteretic Richards' equation model.

This paper is organised as follows: Section 2 provides a brief description of the sand column experiments of Cartwright (2014) and new sand flume experiments which are used for model-data comparison. Section 3 describes the numerical model and boundary conditions. In section 4 the model results are compared with the existing sand column and new sand flume laboratory data. Finally, Section 5 summarises the major findings and conclusions.

2. Laboratory experiments

In this paper, the numerical model FEFLOW (cf. Section 3) is evaluated against observations of the moisture-pressure relationship: firstly in a 1DV context using the sand column data of Cartwright (2014) to facilitate an initial model validation and inter-model comparison (Cartwright, 2014 employed HYDRUS 1D); and secondly in a 2DV context against new sand flume data.

2.1. Sand column experiments

For ease of reference, the sand column experiments of Cartwright (2014) are briefly outlined here. A sand column with 1.6 m height and 0.15 m square was subject to simple harmonic forcing at its base,

$$h_o(t) = d + A\cos(\omega t) \tag{1}$$

where h_o is the driving head [L], d is the mean driving head [L], A is the driving head amplitude [L], $\omega = 2\pi/T$ is the oscillation frequency [T^{-1}], T is the oscillation period [T] and t is the time [T]. During 19 experiments all parameters were kept constant except the oscillation period which varied from 10 s to 12.25 h. A summary of experimental parameters is presented in Table 1. Suction head and moisture content were measured using UMS-T5 tensiometers and MP406 moisture probes at two elevations approximately 0.3 m and 0.5 m above the mean watertable elevation.

2.2. Sand flume experiments

2.2.1. The sand flume

New 2DV experiments were conducted in a sand flume 9 m long, 1.5 m high and 0.14 m wide (cf. Fig. 1). The unconfined sand flume aquifer was forced at one end with a simple harmonic driving head (cf. Eq. (1)) acting across a vertical boundary. No-flow boundaries were applied at the bottom and 'landward' end of flume. The sand surface (top) boundary of the aquifer was covered only with loose plastic to avoid dust settlement whilst still allowing free communication with the atmosphere. The sand surface remained dry for all experiments and thus can be considered a

Table 1
Summary of sand column experimental parameters (Cartwright, 2014).

d (m)	A (m)	T	K_s (m/s)	θ_s (−)	θ_r (−)	α_d (1/m)	β (−)	ζ (−)
0.9	0.16	10 s –12.5 h	2×10^{-4}	0.355	0.03	2.3	10	1.7

d, mean driving head; A, driving head amplitude; T, oscillation period; K_s, saturated hydraulic conductivity; θ_s and θ_r, saturated and residual moisture contents, respectively; α_d and β are the best fit van Genuchten parameters for the first drying curve (after Nielsen and Perrochet, 2000a,b); $\zeta = \alpha_w/\alpha_d$, hysteresis ratio (after Kool and Parker, 1987).

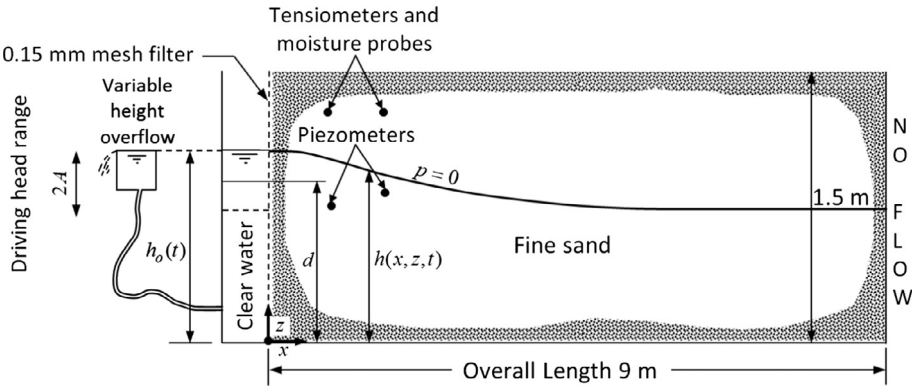

Fig. 1. Schematic illustration of the sand flume (after Cartwright et al., 2003).

no-flow boundary for modelling purposes. For further details of the sand flume the reader is referred to Cartwright et al. (2003).

2.2.2. Moisture-pressure measurements

MP406 moisture probes (2% volumetric moisture content accuracy) were used to measure the moisture content at $z = 1.2$ m at two different horizontal locations along the sand flume ($x = 0.3$ m; 0.75 m). The suction head was observed concurrently at the same locations using UMS T5 tensiometers (±0.5 kPa accuracy). The piezometric head was measured below the watertable using piezometers at the locations $(x, z) = (0.3\text{ m}, 0.7\text{ m})$; $(0.75\text{ m}, 0.8\text{ m})$.

2.2.3. Determination of static moisture retention curves

The static equilibrium drying and wetting curves were measured in situ as follows. For the first drying curve, the water level was set to the sensors' elevation ($z = 1.2$ m) until a static equilibrium in both moisture and pressure was established by monitoring the sensor output. The watertable was then lowered incrementally and both variables were monitored until a new static equilibrium was reached (at least 24 h at each elevation) at which time the moisture content and suction pressure were recorded. This was repeated incrementally down to a minimum watertable elevation of $z = 0.45$ m. The wetting curve was obtained using the same procedure and incrementally raising the watertable. The RECT code (van Genuchten et al., 1991) then was used to determine the best fitting van Genuchten (1980) parameters. The measured moisture-pressure data and the best fit van Genuchten curves are shown in Fig. 2. The summary of hydraulic properties of the sand is summarized in Table 3. As it can be seen, the hysteresis ratio ($\zeta = \alpha_w/\alpha_d$) is 1.65 which is comparable to Kool and Parker's (1987) suggestion ($\zeta \approx 2$) and the value adopted by Cartwright (2014) ($\zeta = 1.7$). α_w and α_d correspond to the van Genuchten parameter α (cf. Eq. (4)) for the wetting and drying curves respectively.

The equivalent saturated height of the unsaturated zone for the sand was estimated based on the first drying curve data (cf. Table 3) according to,

$$H_\psi = \int_0^\infty \frac{\theta - \theta_r}{\theta_s - \theta_r} d\psi \qquad (2)$$

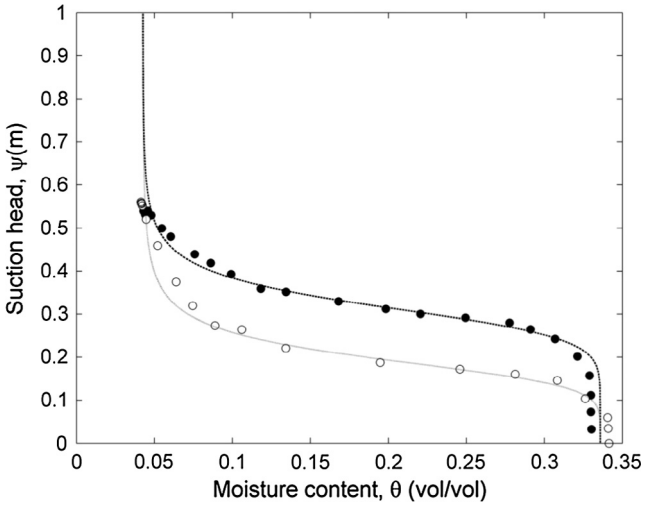

Fig. 2. Main drying and wetting retention curves for the sand used in the sand flume experiments; Symbols show the experimental data for the drying (●) and wetting (○) retention curves and lines show the best van Genuchten curve fit for the drying (bold line) and wetting (thin line) retention curves.

where ψ is the suction head [L], θ is the volumetric moisture content [−], θ_s and θ_r are saturated and residual moisture contents respectively [−] which yields $H_\psi = 0.331$ m.

2.2.4. Oscillating experiments

Five (5) different tests were conducted with different oscillation periods while other parameters (i.e. A and d) were held constant. The sand flume experiment properties are summarized in Table 2.

Each test was initiated with the same procedure to ensure a consistent initial condition for all tests. Before the start of each test,

Table 2
Summary of sand flume experimental parameters.

d (m)	A (m)	T (s)	K_s (m/s)
0.964	0.189	268–2449	4.7×10^{-4}

Table 3
Summary of hydraulic properties of the sand used in the sand flume.

θ_s (vol/vol)	θ_r (vol/vol)	α_d (1/m)	β_d (–)	R_d^2 (–)	α_w (1/m)	β_w (–)	R_w^2 (–)	$\zeta = \alpha_w/\alpha_d$ (–)
0.3358	0.0426	3.1866	8.3508	0.9963	5.2662	5.9610	0.9949	1.6526

θ_s and θ_r, saturated and residual moisture contents, respectively; α and β are the best fit van Genuchten parameters; R^2 is R-squared value for regression of observed versus fitted values; subscript d and w denote parameters for the main drying and wetting retention curves, respectively; $\zeta = \alpha_w/\alpha_d$, hysteresis ratio.

the driving head boundary condition was used as a constant head boundary with the water level set to the sensors' elevation (i.e.$z = 1.2$ m). The aquifer was then allowed to reach a static equilibrium as determined by monitoring the pressure and moisture content sensor output. Once the static equilibrium initial condition was established (at least 24 h), the simple harmonic forcing commenced and the flume was run until a steady oscillatory state was reached in both moisture content and pressure as determined by monitoring both the moisture context and suction pressure time series.

3. Numerical modelling

3.1. Governing equations

Water movement in saturated/unsaturated porous media is commonly described using Richards' (1931) equation,

$$(C_m + S_e S)\frac{\partial \psi}{\partial t} + \nabla \cdot (-K_s k_r(\nabla h)) = 0, \quad h = \psi + z \tag{3}$$

where $h = \psi + z$ is the piezometric head [L], ψ is the pressure head [L], z is the elevation head [L], C_m is the specific moisture capacity [L^{-1}], S_e is the effective saturation [–], S is the storage coefficient [L^{-1}],K_s is the saturated hydraulic conductivity [LT^{-1}], k_r is the relative permeability [–],t is the time [T] and ∇ is the gradient operator.

Here, the soil retention curve properties are described using the van Genuchten's (1980) formulas,

$$\theta = \begin{cases} \theta_r + \frac{\theta_s - \theta_r}{[1+|\alpha\psi|^\beta]^m} & \psi < 0 \\ \theta_s & \psi \geqslant 0 \end{cases} \tag{4}$$

where α [L^{-1}], β [–] and $m = 1 - 1/\beta$ [–] are empirical curve fitting parameters and $h = 0$ is the limit between saturated and unsaturated flow.

The relative permeability is given by,

$$k_r = \begin{cases} S_e^{1/2}\left[1 - (1 - S_e^{1/m})^m\right]^2 & \psi < 0 \\ 1 & \psi \geqslant 0 \end{cases} \tag{5}$$

The effective saturation is,

$$S_e = \frac{\theta - \theta_r}{\theta_s - \theta_r} \tag{6}$$

The specific moisture capacity is defined as,

$$C_m = \frac{d\theta}{d\psi} = \begin{cases} \frac{\alpha m}{1-m}(\theta_s - \theta_r)S_e^{1/m}(1 - S_e^{1/m})^m & \psi < 0 \\ 0 & \psi \geqslant 0 \end{cases} \tag{7}$$

In this paper, FEFLOW 6.0 (FEFLOW, 2012) is used to solve Richards' (1931) equation numerically by the finite element method.

3.2. Seepage face boundary condition

Generally, the rate of fall of the driving head will be faster than the rate the aquifer can drain and so the watertable exit point becomes decoupled from the driving head level and a seepage face is formed. Above the exit point, pressure along the boundary is negative due to meniscus formation and along the seepage face where the watertable is at the sand surface, pressure is at atmospheric pressure ($\psi = 0$).

Shoushtari et al. (2015a) provide a detailed description of the implementation of the seepage face boundary condition in FEFLOW using the prescribed head with flux constraint method. In brief, depending on the flow direction at the boundary, the boundary condition is switched between Dirichlet and Neumann boundary conditions.

3.3. Hysteresis effects

To consider the effects of hysteresis in the numerical model, the empirical scaling model of Scott et al. (1983) was implemented. The drying scanning curves are obtained by using the van Genuchten parameters vector (θ_s^*, θ_r, α_d, β) in Eq. (4), where θ_s^* replaces θ_s, α_d is the van Genuchten parameter for the first drying curve and θ_s^* denotes the saturated moisture content obtained from passing the main drying curve through the reversal point

$$\theta_s^* = (\theta_\Delta - \theta_r)[1 + |\alpha_d \psi_\Delta|^\beta]^m + \theta_r \tag{8}$$

where θ_Δ is the moisture content at the reversal point on the main drying curve at the reversal pressure ψ_Δ.In a similar manner any wetting scanning curve can be obtained by using the van Genuchten parameters vector (θ_s, θ_r^*, α_w, β) in Eq. (4), where α_w is the adopted van Genuchten parameter for the first wetting curve and θ_r^* denotes the residual moisture content obtaining from passing the main wetting curve through the reversal point

$$\theta_r^* = \frac{\theta_s - \theta_\Delta\left[1 + |\alpha_w \psi_\Delta|^\beta\right]^m}{1 - \left[1 + |\alpha_w \psi_\Delta|^\beta\right]^m} \tag{9}$$

where θ_Δ is now the moisture content at the reversal point on the main wetting curve at the reversal pressure ψ_Δ. In this model all scanning loops have the form of Eq. (4). For further details refer to Scott et al. (1983) or Diersch (2014).

3.4. Model discretization

For both the sand column and sand flume models, a 4-noded quadrilateral mesh type with size of 0.01 m × 0.01 m and 0.005 m × 0.005 m respectively was used for simulations. A preliminary model sensitivity analysis to mesh size showed that the model results are independent of the mesh size at this resolution. The adopted mesh resolutions are also consistent with other Richards' equation models applied to similar oscillating systems (e.g. Clement et al., 1996; Lehmann et al., 1998; Ataie-Ashtiani et al., 1999; Nielsen and Perrochet, 2000a,b; Werner and Lockington, 2003).

4. Results and discussions

4.1. Sand column model-data comparison

The sand column data of Cartwright (2014) was used for the initial model-data and inter-model comparisons (Cartwright (2014)

used Hydrus1D). Consistent with Cartwright (2014), a hysteresis ratio of $\zeta = \alpha_w/\alpha_d \approx 1.7$ (Kool and Parker, 1987) was adopted for the hysteretic model where the drying curve value α_d corresponds to the measured value given in Table 1.

Fig. 3 shows the model-data comparison of moisture-pressure relationships at $z = 1.2$ m and $z = 1.4$ m for different oscillation periods. Although there are some quantitative differences between the model and data, the model captures the general behaviour of the observed moisture-pressure dynamics. This is namely, the size of hysteresis loops decreasing with decreasing oscillation period and the scanning loops becoming non-hysteretic for the shorter periods. Table 4 summarizes the measured and simulated moisture content and suction head range for different periods at $z = 1.2; 1.4$ m. Generally, the model underestimates both moisture and pressure range in comparison with the measured data especially for $z = 1.4$ m. The present FEFLOW model results are very similar to those obtained using the HYDRUS 1D model by Cartwright (2014).

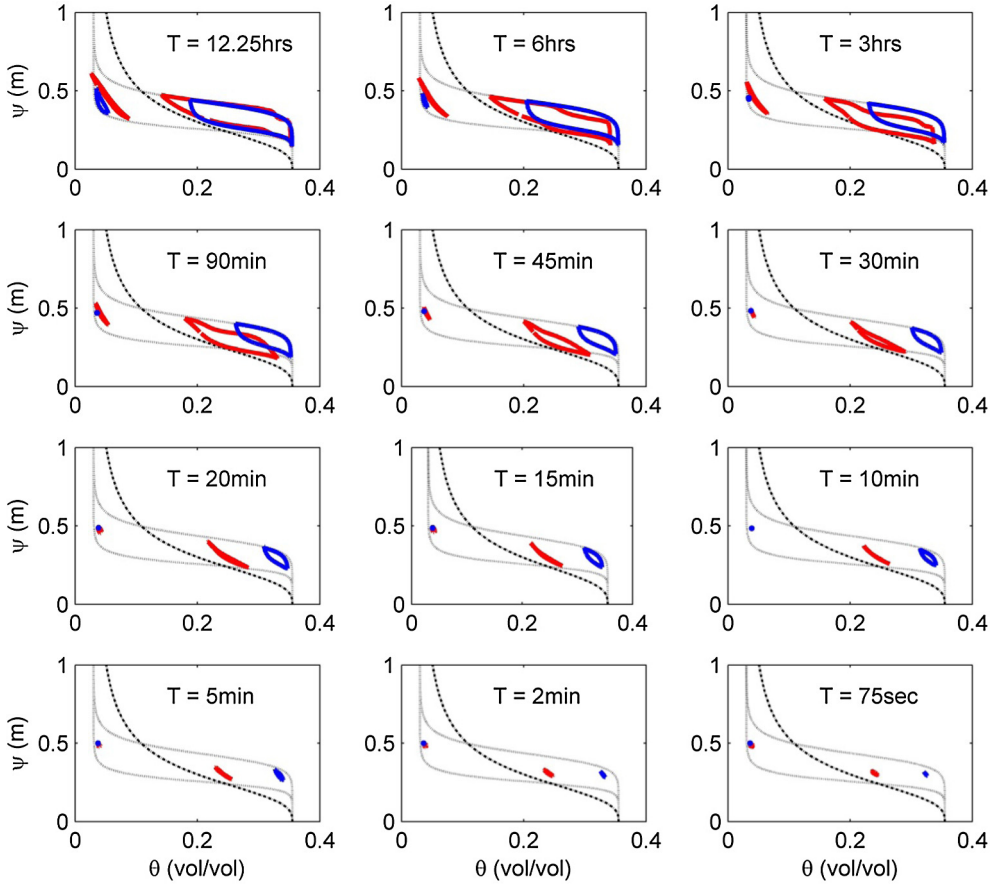

Fig. 3. Comparison of measured data of Cartwright (2014) (solid red lines) and simulated (solid blue lines) moisture-pressure relationships at $z = 1.2$ m and $z = 1.4$ m for different oscillation periods. The thin lines denote the equilibrium van Genuchten (1980) curves (drying and wetting) based on parameters given in Table 1. The doted curve is an indicative van Genuchten (1980) curve with $\alpha = \alpha_w = 3.91\ m^{-1}$ and $\beta = 3$. (For interpretation of the references to colour in this figure legend, the reader is referred to the web version of this article.)

Table 4
Measured and simulated moisture and suction head range in the 1DV sand column.

T	$z = 1.2$ m				$z = 1.4$ m			
	θ_{range} (vol/vol)		ψ_{range} (m)		θ_{range} (vol/vol)		ψ_{range} (m)	
	Data	Model	Data	Model	Data	Model	Data	Model
12.25 h	0.211	0.166	0.291	0.298	0.062	0.020	0.288	0.157
6 h	0.197	0.149	0.305	0.280	0.047	0.008	0.245	0.087
90 min	0.180	0.121	0.288	0.249	0.034	0.000	0.199	0.008
45 min	0.151	0.089	0.252	0.210	0.020	0.000	0.136	0.000
30 min	0.108	0.061	0.214	0.175	0.010	0.000	0.075	0.000
20 min	0.088	0.048	0.189	0.151	0.006	0.000	0.050	0.000
15 min	0.065	0.038	0.163	0.132	0.003	0.000	0.026	0.000
10 min	0.057	0.032	0.145	0.116	0.002	0.000	0.016	0.000
5 min	0.042	0.026	0.116	0.098	0.001	0.000	0.007	0.000
2 min	0.027	0.013	0.075	0.061	0.000	0.000	0.001	0.000
75 s	0.013	0.007	0.037	0.035	0.001	0.000	0.001	0.000

4.2. Sand flume model-data comparison

4.2.1. Moisture-pressure scanning loops

Fig. 4 and 5 respectively show the measured and simulated scanning loops in the sand flume at the two monitoring locations for each of the 5 different oscillation periods. The measured equilibrium van Genuchten (1980) curves (drying and wetting) (cf. Table 3) are also shown in these figures for reference. It should be noted that the saturated moisture content (θ_s) has been adjusted based on the maximum moisture content measured in the dynamic test for the longest period (i.e. $T = 2449$ s); hence $\theta_s = 0.303$ (vol/vol) was used to compute the main drying and

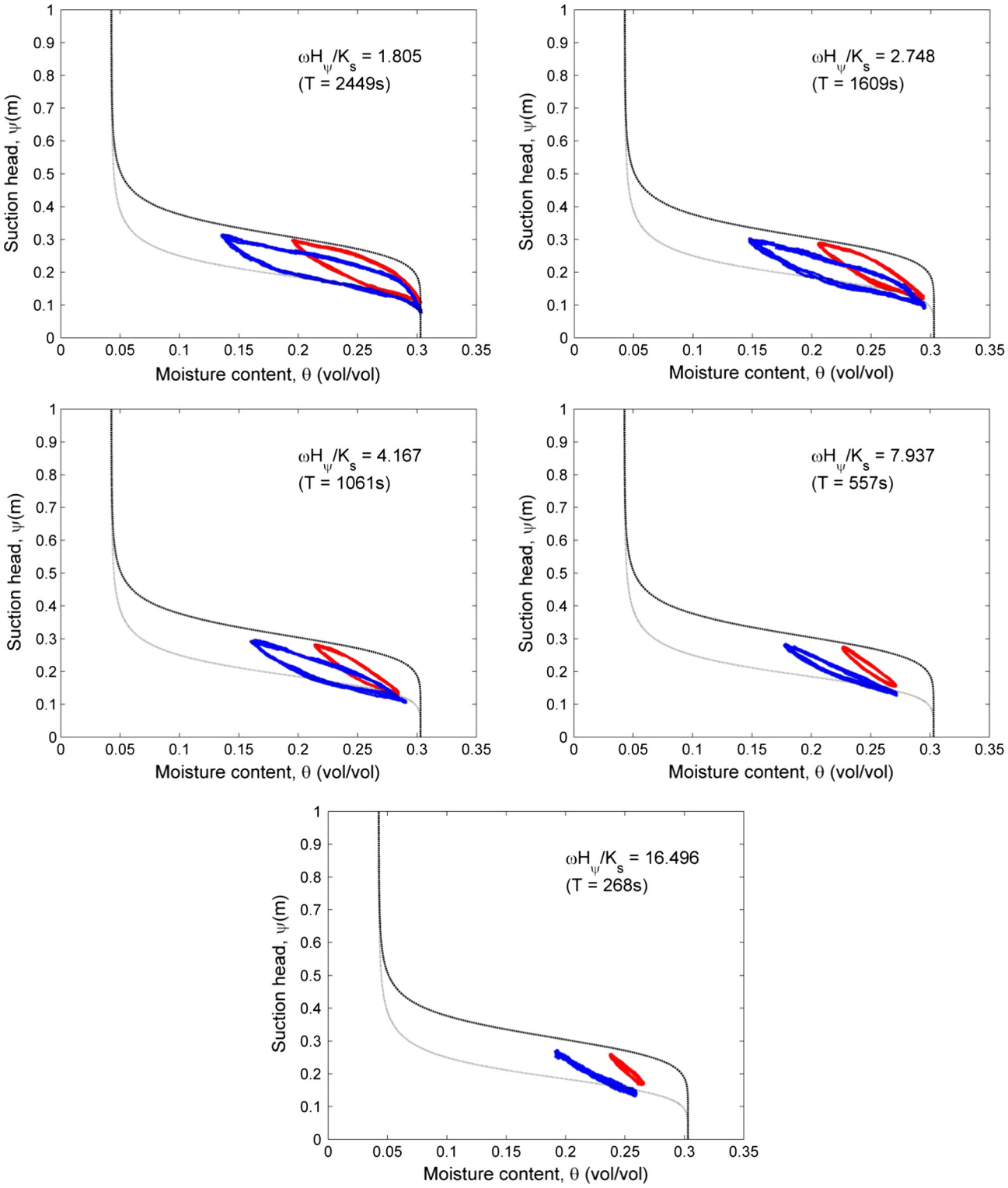

Fig. 4. Measured scanning loops in the sand flume at $z = 1.2$ m for different locations $x = 0.3$ m (blue line) and $x = 0.75$ m (red line) for different oscillation periods. The bold and thin lines denote the equilibrium van Genuchten (1980) curves (drying and wetting) based on parameters given in Table 3. Note: the saturated moisture content was adjusted based on the maximum measured moisture content for the longest period (i.e. $T = 2449$ s), hence $\theta_s = 0.303$ (vol/vol) was used to obtain the main drying and wetting curves. (For interpretation of the references to colour in this figure legend, the reader is referred to the web version of this article.)

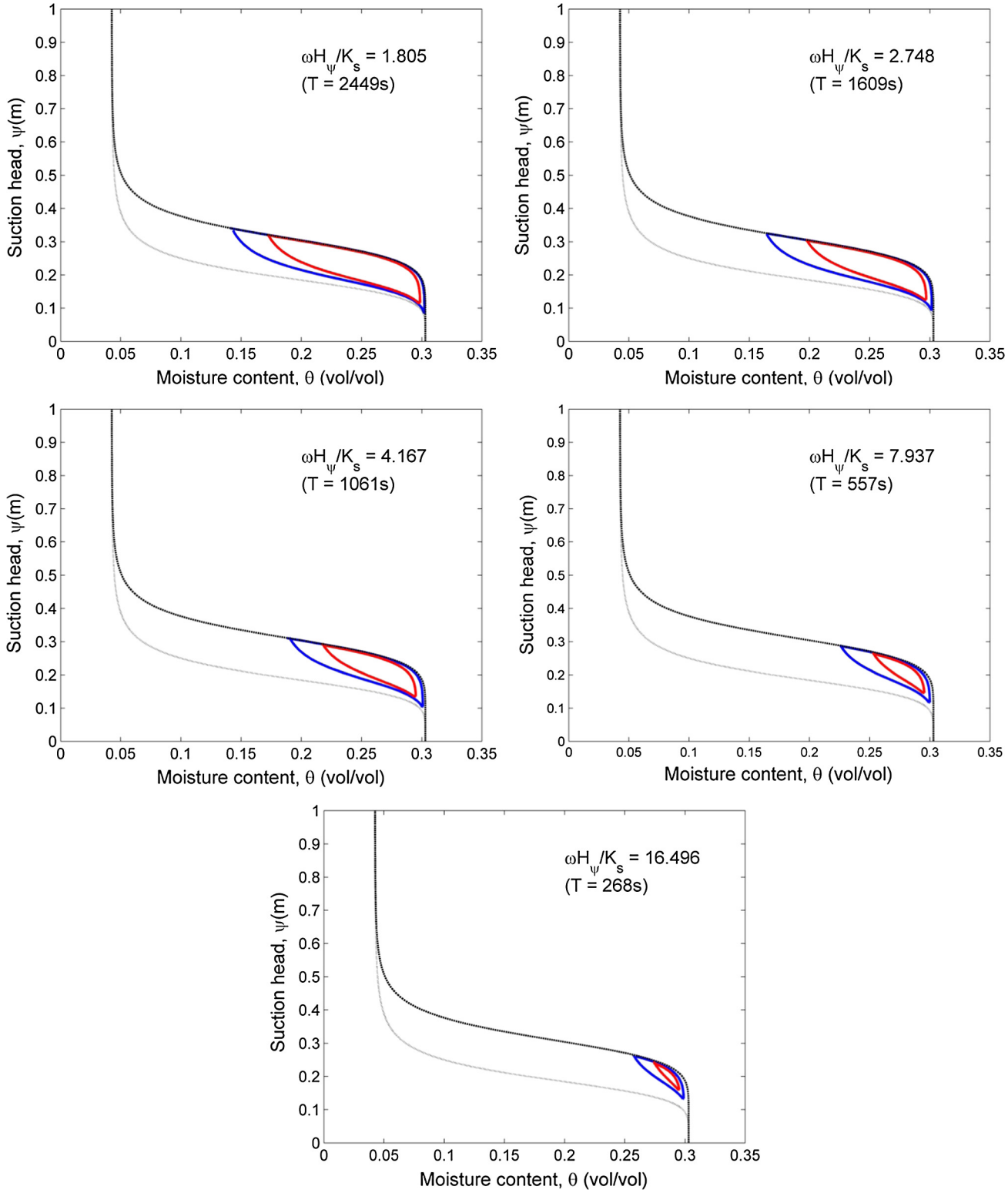

Fig. 5. Simulated scanning loops in the sand flume at $z = 1.2$ m for different locations $x = 0.3$ m (blue line) and $x = 0.75$ m (red line) for different oscillation periods. Descriptions as per Fig. 4. (For interpretation of the references to colour in this figure legend, the reader is referred to the web version of this article.)

wetting curves for modelling purposes (respectively the bold and thin lines in Figs. 4 and 5).

The size of the observed hysteresis loop becomes smaller with increasing distance from the driving head and also with decreasing oscillation period. This is consistent with (a) the decay of the watertable wave with distance from the forcing and (b) a faster decay rate for shorter period oscillations (e.g. Shoushtari et al., 2016). The moisture-pressure dynamics start to exhibit non-hysteretic behaviour for the shortest period (i.e. $T = 268$ s) but with a qualitatively different capillary capacity compared to that

of the static equilibrium moisture retention curves. This finding is consistent with the sand column data of Cartwright (2014) for $T < 15$ min (see Fig. 3).

The model qualitatively reproduces the nature of the scanning loops however there are discrepancies in the location of loops predicted by model. The model tends to predict wetter scanning loops than is observed, particularly as the oscillation frequency decreases. A model sensitivity analysis was conducted in an attempt to better calibrate the model however changes in the adopted van Genuchten parameters only led to an up or down shift in the scanning loops (i.e. changing suction pressure) and not the required horizontal shift (i.e. changing moisture content). A possible explanation for the discrepancy is due to the influence of oscillation period on the response of both the watertable wave and the unsaturated zone. Firstly, longer period waves decay slower and so the watertable wave amplitude at a given x location will be larger than a shorter period wave. Second, in the case of longer period waves, the unsaturated zone has more time to respond to the underlying wave motion and the tension saturated zone periodically moves higher in the aquifer. The net result is that (at least at the $z = 1.2$ m elevation used in the present experiments), the longer period oscillations leads to a wetter scanning loop. As the oscillation period decreases, both the watertable wave amplitude decreases and so does the unsaturated zone response leading to an overall drying of the loops. The reason that this is not captured to the same extent in the model is due to the fact that it is unable to accurately predict the amplitude decay, particularly for the shorter oscillation periods as previously demonstrated by Shoushtari et al. (2016).

4.2.2. Oscillation range: pore pressure and moisture content

The measured and simulated oscillation range of all variable (saturated zone piezometric head and unsaturated zone suction head and moisture content) as a function of oscillation period are presented in Fig. 6. The range of all variables increase with increasing oscillation period (i.e. solid squares and circles for $x = 0.3$ m and open squares and circles for $x = 0.75$ m in Fig. 6) consistent with the increasing the size of scanning loops (Figs. 4 and 5). The model-data comparison in terms of the oscillation range and damping of the saturated zone piezometric head and unsaturated zone suction head and moisture content is quantified in Table 5. The model reproduces the measured data with accuracy in a range of 2–15% for piezometric head range, −10% to +16% for suction head range and −18% to 38% for moisture content range.

The relative damping was calculated as the difference in oscillation range between the two horizontal locations normalised by the

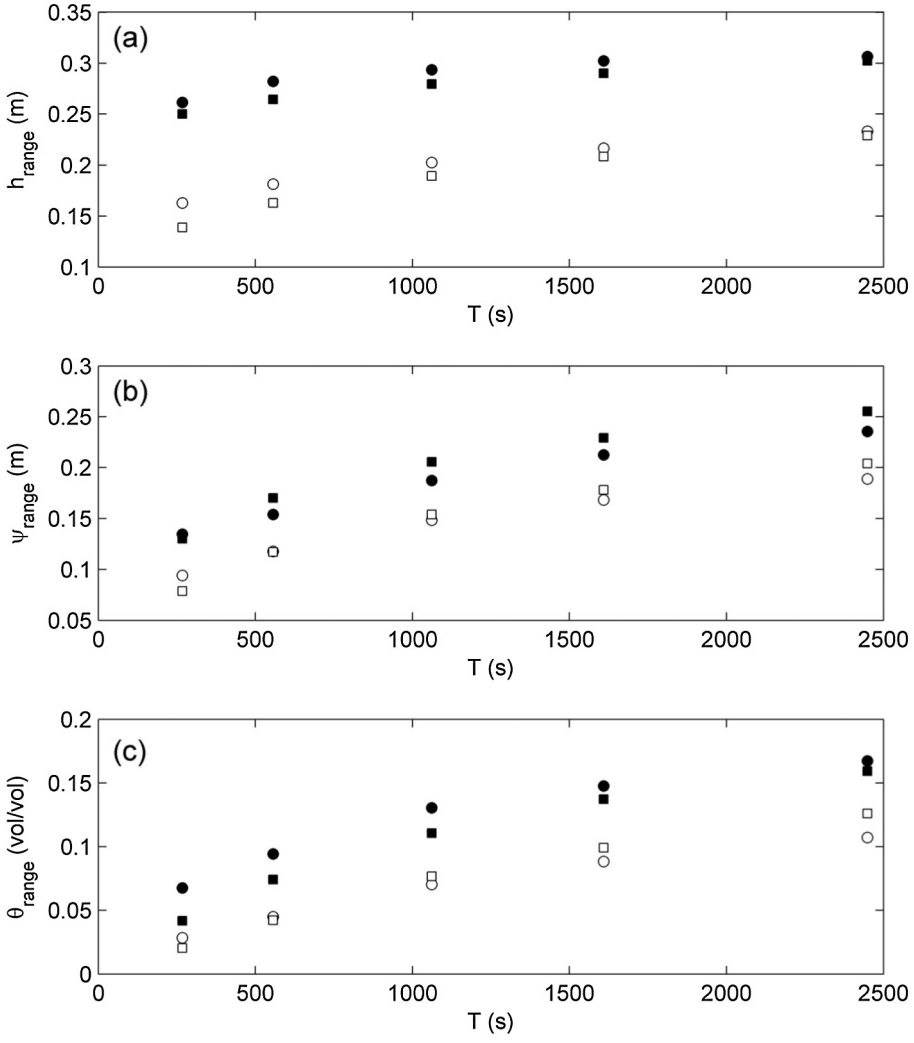

Fig. 6. Measured (circles) and simulated (squares) data range of (a) piezometric head in the saturated part at $(x,z) = (0.3\text{ m},0.7\text{ m})$ (solid symbols) and $(x,z) = (0.75\text{ m},0.8\text{ m})$ (open symbols), (b) suction head in the unsaturated part at and $(x,z) = (0.3\text{ m},1.2\text{ m})$ (solid symbols) and $(x,z) = (0.75\text{ m},1.2\text{ m})$ (open symbols) and (c) moisture content at $(x,z) = (0.3\text{ m},1.2\text{ m})$ (solid symbols) and $(x,z) = (0.75\text{ m},1.2\text{ m})$ (open symbols) respect to the oscillation period.

oscillation range at $x = 0.3$ m and expressed as a percentage. All three variables exhibit an increase in relative damping with decreasing oscillation period consistent with the behaviour of a decaying watertable wave (e.g. Shoushtari et al., 2016). Of particular interest is that the relative damping of the suction head is less than the saturated zone piezometric head. This is due to the fact that the damping rate is inversely related to the hydraulic conductivity (e.g. Nielsen, 1990) and the mean hydraulic conductivity at $x = 0.75$ m is greater than at $x = 0.3$ m (as inferred from Fig. 4 which shows that the mean moisture content is higher at $x = 0.75$ m). That is, the mean moisture content at $z = 1.2$ m is observed to increase with distance landward, hence the mean hydraulic conductivity increases leading to a reduction in the pressure fluctuation decay rate.

The relative damping of the moisture content is higher than the suction head consistent with the fact that transmission of pressure through a porous medium is easier than mass transfer. This is not dissimilar to the case where the dynamic response of the salinity distribution (mass transfer) in coastal aquifers is less than the dynamic response of the watertable (pressure transfer) to tidal forcing (e.g. Ataie-Ashtiani et al., 1999; Cartwright et al., 2004; Robinson et al., 2006).

Table 5
The summary of measured and simulated range and relative damping for the saturated zone piezometric head (h), suction head (ψ) and moisture content (θ) in the sand flume.

	$x = 0.3$ m (1)			$x = 0.75$ m (2)			Damping (3) = 100 × [(1) − (2)]/(1)		
$T(s)$	h_{range} (m)	ψ_{range} (m)	θ_{range} (vol/vol)	h_{range} (m)	ψ_{range} (m)	θ_{range} (vol/vol)	h_{range} (%)	ψ_{range} (%)	θ_{range} (%)
Data									
2449	0.307	0.236	0.167	0.233	0.189	0.107	24.10	19.92	35.93
1609	0.302	0.213	0.148	0.217	0.168	0.088	28.15	21.13	40.54
1061	0.294	0.187	0.130	0.202	0.148	0.070	31.29	20.86	46.15
557	0.282	0.154	0.094	0.181	0.118	0.045	35.82	23.38	52.13
268	0.262	0.135	0.068	0.163	0.094	0.028	37.79	30.37	58.82
Model									
2449	0.302	0.255	0.159	0.229	0.204	0.126	24.17	20.00	20.75
1609	0.290	0.229	0.137	0.208	0.178	0.099	28.28	22.27	27.74
1061	0.279	0.206	0.111	0.189	0.154	0.077	32.26	25.24	30.63
557	0.264	0.170	0.074	0.163	0.117	0.042	38.26	31.18	43.24
268	0.250	0.130	0.042	0.139	0.079	0.021	44.40	39.23	50.00

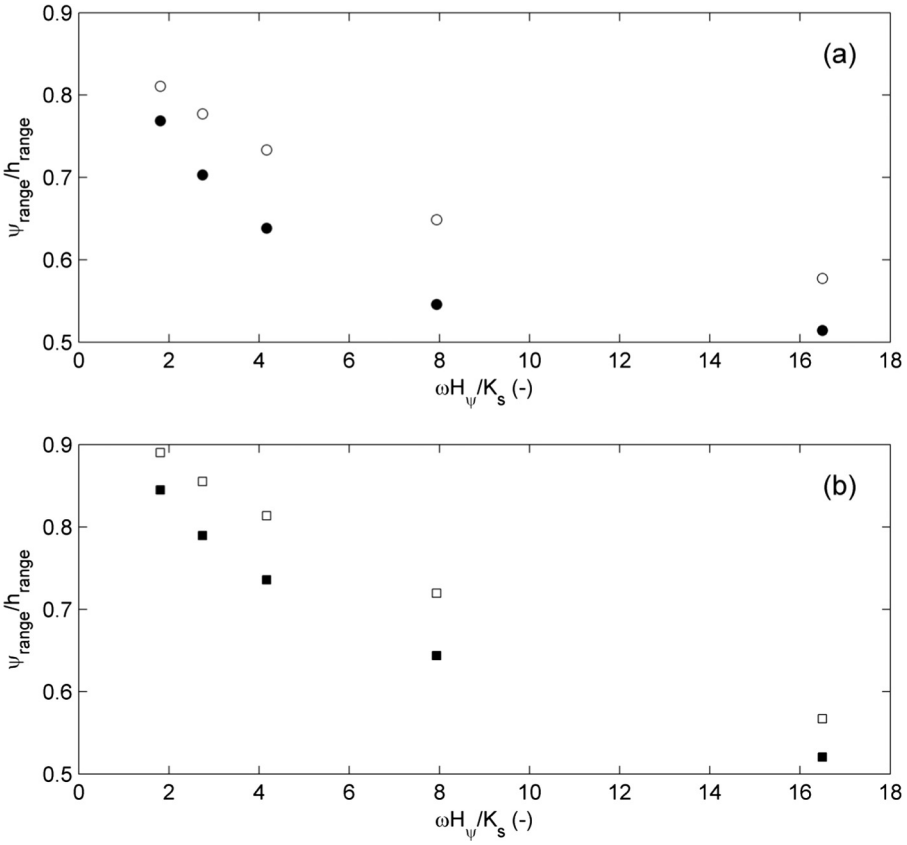

Fig. 7. Measured (circles) (a) and simulated (squares) (b) data of the ratio of suction head range to piezometric head range (i.e. ψ_{range}/h_{range}) at $x = 0.3$ m (solid symbols) and at $x = 0.75$ m (open symbols) respect to dimensionless frequency, $\omega H_\psi/K_s$. Parameters used were $H_\psi = 0.331$ m and $K_s = 4.7 \times 10^{-4}$ (m/s).

4.2.3. Pressure fluctuation decay characteristics

To further examine the difference in pressure fluctuation decay characteristics between the saturated and unsaturated zones, the ratios of unsaturated suction head range and saturated zone piezometric head range (ψ_{range}/h_{range}) are presented in Fig. 7(a) and (b). The ratios are presented with respect to the dimensionless frequency $\omega H_\psi/K_s$, where ω is the angular frequency, H_ψ is the equivalent saturated height of the unsaturated zone (cf. Eq. (2)) and K_s is the saturated hydraulic conductivity (cf. Table 2).

At both locations, the ratio ψ_{range}/h_{range} decreases with increasing $\omega H_\psi/K_s$ (i.e. decreasing oscillation period, T). This indicates that, with decreasing oscillation period, the rate of decay in the unsaturated zone increases more than in the saturated zone. This is consistent with the fact that the time scale for the unsaturated zone to adjust to watertable motion is greater than the saturated zone pressure. Fig. 7 also shows that the ratio is greater at $x = 0.75$ m than $x = 0.3$ m consistent with an unsaturated zone damping rate which decreases further landward as discussed above.

4.2.4. Harmonic analysis

To examine the existence of any higher harmonic generation, the amplitudes and phases of both the measured and simulated data were extracted using harmonic analysis with the harmonic components summarized in Table 6. The value of the third harmonic amplitude was found to be insignificant ($R_3 \leqslant 0.004$ m) and has been excluded from the analysis.

The ratio of the second harmonic amplitude to the fundamental mode (R_2/R_1) indicates the relative significance of higher harmonics. Noting that the second harmonic in the sand flume driving head is of the order 10% of the primary harmonic and, as such, there is no evidence of higher harmonic generation in the interior of the sand flume in either the saturated or unsaturated zones where the observed $R_2/R_1 < 10\%$ for all locations and parameters.

In the case of the model however (where the driving head is purely simple harmonic,$R_2/R_1 = 0$), there is evidence of the generation of higher harmonics, particularly in the unsaturated zone. This model-data discrepancy is the likely the result of the model being unable to predict the absolute positions of the measured scanning loops (cf. Figs. 4 and 5). The laboratory data shows a reduction in the maximum saturation with decreasing oscillation period while the simulated scanning loops remain closer to saturated conditions for all periods.

The phase lag for the first harmonic in each of the variables (h, ψ and θ) at (x, z) with respect to the first harmonic of the driving head at (i.e. ϕ_{o1}) is shown in Table 6. Both the flume data and model show an increasing phase lag with increasing distance landward and with higher elevation with respect to the driving head. In

Table 6
The summary of measured and simulated ratio of the second harmonic amplitude to the fundamental mode (R_2/R_1) and the phase lag for the first harmonic phase respect to the first harmonic phase of driving head ($\phi_1 - \phi_{o1}$) for saturated zone piezometric head (h), suction head (ψ) and moisture content (θ).

			Data		Model	
	x (m)	z (m)	R_2/R_1 (–)	$\phi_1 - \phi_{o1}$ (rad)	R_2/R_1 (–)	$\phi_1 - \phi_{o1}$ (rad)
$T = 2449$ s						
h	0.00	0.00	0.104	0.000	0.000	0.000
	0.30	0.70	0.081	0.105	0.029	0.349
	0.75	0.80	0.080	0.266	0.040	0.521
ψ	0.30	1.20	0.061	0.384	0.104	0.571
	0.75	1.20	0.072	0.464	0.070	0.694
θ	0.30	1.20	0.004	0.682	0.170	0.994
	0.75	1.20	0.030	0.829	0.136	1.145
$T = 1609$ s						
h	0.00	0.00	0.102	0.000	0.001	0.000
	0.30	0.70	0.093	0.100	0.031	0.352
	0.75	0.80	0.077	0.282	0.044	0.538
ψ	0.30	1.20	0.032	0.447	0.115	0.619
	0.75	1.20	0.063	0.518	0.076	0.753
θ	0.30	1.20	0.060	0.733	0.176	1.055
	0.75	1.20	0.051	0.863	0.135	1.198
$T = 1061$ s						
h	0.00	0.00	0.108	0.000	0.000	0.000
	0.30	0.70	0.109	0.115	0.038	0.356
	0.75	0.80	0.076	0.301	0.053	0.554
ψ	0.30	1.20	0.064	0.529	0.136	0.677
	0.75	1.20	0.052	0.590	0.089	0.819
θ	0.30	1.20	0.094	0.796	0.175	1.126
	0.75	1.20	0.085	0.878	0.131	1.251
$T = 557$ s						
h	0.00	0.00	0.103	0.000	0.000	0.000
	0.30	0.70	0.064	0.138	0.043	0.112
	0.75	0.80	0.049	0.325	0.058	0.317
ψ	0.30	1.20	0.066	0.654	0.157	0.521
	0.75	1.20	0.057	0.685	0.097	0.675
θ	0.30	1.20	0.106	0.832	0.164	0.959
	0.75	1.20	0.076	0.894	0.129	1.045
$T = 268$ s						
h	0.00	0.00	0.100	0.000	0.002	0.000
	0.30	0.70	0.071	0.121	0.040	0.095
	0.75	0.80	0.067	0.317	0.049	0.289
ψ	0.30	1.20	0.046	0.908	0.160	0.594
	0.75	1.20	0.029	0.824	0.091	0.779
θ	0.30	1.20	0.095	0.851	0.132	0.992
	0.75	1.20	0.070	0.985	0.105	1.061

addition, in both data and model, there is a phase lag between suction head and moisture content at the same location indicating that moisture content has a larger response time in adjusting to the underlying watertable.

5. Conclusion

New sand flume experiments have been conducted to examine the influence of oscillation period on 2DV moisture-pressure dynamics above a progressive watertable wave in an unconfined aquifer. With the exception of the shortest period measured, the data clearly show the formation of hysteretic scanning loops in the unsaturated zone with the size of the loops decreasing with both decreasing oscillation period and increasing distance from the driving head boundary consistent with the dispersion of the underlying watertable wave. At the shortest period ($T = 268$ s), the scanning "loop" is a single valued curve indicating non-hysteretic behaviour at the higher frequency. This observation is consistent with the observed moisture-pressure dynamics in the 1DV sand column experiments of Cartwright (2014). It is noted that, in both the 1DV and 2DV cases, the overall slope of the non-hysteretic scanning loop (the capillary capacity) is qualitatively different to the measured static equilibrium wetting and drying curves. This provides some insight into (a) why existing non-hysteretic models using static equilibrium curves have been unable to reproduce sand column observations (e.g. Werner and Lockington, 2003; Cartwright et al., 2005) and (b) why modelled hysteresis appears to have little effect on the dispersion of watertable waves (cf. Shoushtari et al., 2015b).

The scanning loops were observed to become drier with decreasing oscillation period. It is suggested that this is due, at least in part, to the fact that in the case of longer period waves (a) the watertable wave decay is slower (hence the wave amplitude is larger) and (b) the unsaturated zone (moisture content) has more time to respond to the underlying watertable motion. The net result is an increase in the mean moisture content in the unsaturated zone with distance landward (at least at the $z = 1.2$ m elevation used in the experiments).

The data was further analysed by extracting the oscillation range and relative damping for each of the piezometric head, suction head and moisture content. The relative damping of the suction head is less than the saturated zone piezometric head which is likely due to the fact that the mean moisture content (and hence hydraulic conductivity) was observed to increase with landward distance. The relative damping of the moisture content is the highest of all variables consistent with the idea that transmission of pressure through a porous medium occurs more readily than mass transfer.

Harmonic analysis of the time series revealed that there was no observable generation of higher harmonics in any variable. The phase lag between all variables (piezometric head, suction head and moisture content) and the driving head increased with increasing distance landward and elevation in the aquifer. In addition, a phase lag exists between the suction head and moisture content measured at the same location, indicating more time is needed for the moisture content to respond to watertable fluctuations than the suction head.

The new data facilitated the evaluation of a numerical solution of a hysteretic Richards' equation model. The simulated scanning loops showed some of the same qualitative behaviour as observed in the data. In terms of oscillation ranges, the model can reproduce the measured data with accuracy of 2–15% (saturated zone piezometric head), −10% to16% (suction head) and −18% to 38% (moisture content). Whilst the model performed reasonably well in terms of the observed dynamic ranges, it was unable to predict the absolute positions of the scanning loops with the model predicting wetter loops than is observed, particularly at higher frequencies. Varying the model van Genuchten parameters only resulted in shifting the loops up and down (i.e. different suction head) and not horizontally as required to better match the data. The discrepancy is likely due to the inability of the model to accurately predict the watertable wave dispersion, particularly at higher frequencies (Shoushtari et al., 2016).

In summary, there is a need for further research into the ability of Richards' equation models to predict watertable wave dispersion at higher oscillation frequencies. Also, whilst moisture-pressure dynamics have been shown to be non-hysteretic at higher frequencies, the nature of the relationship (and hence the capillary capacity) is qualitatively different to the static equilibrium curves hence the need for hysteresis algorithms (which allow for deviation away from the static curves) or an alternative non-hysteric relationship that better represents the observed dynamic relationship (cf. the "magical" $\beta = 3$ curve described by Cartwright et al., 2005).

Acknowledgements

The first author has been supported by Griffith University International Postgraduate Research Scholarship (GUIPRS) and Griffith University Postgraduate Research Scholarship (GUPRS). The authors also acknowledge the valuable comments received during the review process.

References

Ataie-Ashtiani, B., Volker, R.E., Lockington, D.A., 1999. Numerical and experimental study of seepage in unconfined aquifers with a periodic boundary condition. J. Hydrol. 222 (1–4), 165–184. 13.

Bakhtyar, R., Brovelli, A., Barry, D.A., Li, L., 2011. Wave-induced watertable fluctuations, sediment transport and beach profile change: modeling and comparison with large-scale laboratory experiments. Coast. Eng. 58 (1), 103–118.

Barry, D.A., Barry, S.J., Parlange, J.-Y., 1996. Capillarity correction to periodic solutions of the shallow flow approximation. In: Pattiaratchi, C.B. (Ed.), Mixing in Estuaries and Coastal Seas, Coastal and Estuarine Studies. AGU, Washington, DC, pp. 496–510.

Brooks, R.H., Corey, A.T., 1966. Properties of porous media affecting fluid flow. J. Irrig. Drain. Div., ASCE 92_IR2, 61–88.

Cartwright, N., Nielsen, P., Dunn, S.L., 2003. Watertable waves in an unconfined aquifer: experiments and modeling. Water Resour. Res. 39 (12), 1330–1342.

Cartwright, N., Li, L., Nielsen, P., 2004. Response of the salt-freshwater interface in a coastal aquifer to a wave-induced groundwater pulse: field observations and modelling. Adv. Water Resour. 27 (3), 297–303.

Cartwright, N., Nielsen, P., Perrochet, P., 2005. The influence of capillarity on a simple harmonic oscillating watertable: sand column experiments and modelling. Water Resour. Res. 41 (8), W08416.

Cartwright, N., 2014. Moisture-pressure dynamics above an oscillating watertable. J. Hydrol. 512, 442–446.

Clement, T.P., Wise, W.R., Molz, F.J., 1994. A physically based, two-dimensional, finite-difference algorithm for modelling variably saturated flow. J. Hydrol. 161, 71–90.

Clement, T.P., Wise, W.R., Molz, F.J., Wen, M., 1996. A comparison of modeling approaches for steady-state unconfined flow. J. Hydrol. 161, 189–209.

Diersch, H.-J.G., 2014. FEFLOW - Finite Element Modeling of Flow, Mass and Heat Transport in Porous and Fractured Media, vol. XXXV. Springer, Berlin Heidelberg, p. 996. ISBN 978-3-642-38738-8, ISBN 978-3-642-38739-5 (eBook).

Emery, K.O., Foster, J.F., 1948. Water tables in marine beaches. J. Mar. Res. 7, 644–654.

FEFLOW, 2012. Finite Element Subsurface Flow and Transport Simulation System. User Manual Version 6.0, 116.

Grant, U.S., 1946. Effects of groundwater table on beach erosion. Geol. Soc. Am. Bull. 57, 1952 (abstract).

Grant, U.S., 1948. Influence of the water table on beach aggradation and degradation. J. Mar. Res. 7, 655–660.

Green, W.H., Ampt, G.A., 1911. Studies on soil physics 1. The flow of air and water through soils. J. Agric. Sci. IV (I), 1–24.

Heiss, J.W., Ullman, W.J., Michael, H.A., 2014. Swash zone moisture dynamics and unsaturated infiltration in two sandy beach aquifers. Estuarine Coastal Shelf Sci. 143, 20–31. http://dx.doi.org/10.1016/j.ecss.2014.03.015.

Kool, J.B., Parker, J.C., 1987. Development and evaluation of closed-form expressions for hysteretic soil hydraulic properties. Water Resour. Res. 23 (1), 105–114.

Lehmann, P., Stauffer, F., Hinz, C., Dury, O., Flühler, H., 1998. Effect of hysteresis on water flow in a sand column with a fluctuating capillary fringe. J. Contam. Hydrol. 33, 81–100.
Li, L., Barry, D.A., Stagnitti, F., Parlange, J.-Y., 2000. Groundwater waves in a coastal aquifer: a new governing equation including vertical effects and capillarity. Water Resour. Res. 36 (2), 411–420.
Mualem, Y., 1984. A modified dependent-domain theory of hysteresis. Soil Sci. 137_5, 283–291.
Nielsen, P., 1990. Tidal dynamics of the watertable in beaches. Water Resour. Res. 26, 2127–2134.
Nielsen, P., Perrochet, P., 2000a. Watertable dynamics under capillary fringes: experiments and modeling. Adv. Water Resour. 23, 503–515.
Nielsen, P., Perrochet, P., 2000b. ERRATA: watertable dynamics under capillary fringes: experiments and modelling [Adv. Water Resour. 23 (2000) 503–515]. Adv. Water Resour. 23, 907–908.
Parker, J.C., Lenhard, R.J., 1987. A model for hysteretic constitutive relations governing multiphase flow. 1. Saturation–pressure relations. Water Resour. Res. 23, 2187–2196.
Richards, L.A., 1931. Capillary conduction of liquids through porous mediums. Physics 1 (5), 318–333.
Robinson, C., Gibbes, B., Li, L., 2006. Driving mechanisms for groundwater flow and salt transport in a subterranean estuary. Geophys. Res. Lett. 33 (3), L03402. http://dx.doi.org/10.1029/2005GL025247.
Scott, P.S., Farquhar, G.J., Kouwen, N., 1983. Hysteresis effects on net infiltration. Advances in Infiltration. Am. Soc. Agric. Eng. 11–83, 163–170.
Shoushtari, S.M.H.J., Nielsen, P., Cartwright, N., Perrochet, P., 2015a. Periodic seepage face formation and water pressure distribution along a vertical boundary of an aquifer. J. Hydrol. 523, 24–33.
Shoushtari, S.M.H.J., Cartwright, N., Perrochet, P., Nielsen, P., 2015b. Influence of hysteresis on groundwater wave dynamics in an unconfined aquifer with a sloping boundary. J. Hydrol. 531, 1114–1121.
Shoushtari, S.M.H.J., Cartwright, N., Perrochet, P., Nielsen, P., 2016. The effects of oscillation period on groundwater wave dispersion in a sandy unconfined aquifer: sand flume experiments and modelling. J. Hydrol. 533, 412–440.
Šimůnek, J., Šejna, M., van Genuchten, M.T., 1998. The HYDRUS-1D Software Package for Simulating the Movement of Water, Heat, and Multiple Solutes in Variably Saturated Media, Version 2.0. US Salinity Laboratory, ARS, USDA, Riverside, California, p. 178.
Stauffer, F., 1996. Hysterestic unsaturated flow modelling. In: Proceedings of the Second International Conference on Hydroinformatics, Hydroinformatics '96, Zu¨Rich, Switzerland. Balkema, Rotterdam, pp. 589–595.
Stauffer, F., Kinzelbach, W., 2001. Cyclic hysteretic flow in porous medium column: model, experiment, and simulations. J. Hydrol. 240 (3–4), 264–275.
van Genuchten, M.T., 1980. A closed form equation for predicting the hydraulic conductivity of unsaturated soils. Soil Sci. Soc. Am. J. 44, 892–898.
van Genuchten, M.Th., Leij, F.J., Yates, S.R., 1991. The RETC Code for Quantifying the Hydraulic Functions of Unsaturated Soils, Version 1.0 EPA Report 600/2-91/065. U.S. Salinity Laboratory, USDA, ARS, Riverside, California.
Werner, A.D., Lockington, D.A., 2003. Influence of hysteresis on tidal capillary fringe dynamics in a well-sorted sand. Adv. Water Resour. 26 (11), 1199–1204.
Xin, P., Robinson, C., Li, L., Barry, D.A., Bakhtyar, R., 2010. Effects of wave forcing on asubterranean estuary. Water Resour. Res. 46 (W12505). http://dx.doi.org/10.1029/2010WR009632.